

A Simulation of the Circulation in the Gulf of Mexico

Alan F. Blumberg and George L. Mellor¹

Dynalysis of Princeton, 219 Wall Street, Princeton, New Jersey 08540-1512; and also ¹Geophysical Fluid Dynamics Program, Princeton University, Princeton, New Jersey 08544, USA

Abstract

The monthly climatology of the surface wind stress and heat flux and the seasonal climatology of the hydrography of the Gulf of Mexico have been created. These data provide the surface forcing, lateral boundary conditions and initialization for a $\frac{1}{2}^\circ \times \frac{1}{2}^\circ$, 16-level, three-dimensional, time-dependent numerical model of the Gulf. An analytical second moment turbulence closure scheme embedded within the circulation model provides for surface-mixed layer dynamics. The computational code uses a split-mode time marching procedure to include a free surface at minimal sacrifice in computer cost compared to rigid lid models. A year's simulation was obtained utilizing a two-component wind model which satisfies both synoptic surface mixing and climatological general circulation requirements. Comparison of the three-dimensional model results with observational data indicates that the model can reproduce many aspects of the large-scale features of the circulation. The seasonal cycle of the mixed layer and thermocline compares well, but not perfectly, with climatology. An area-averaged, one-dimensional ($z-t$) model and a reduced-gravity, two-dimensional ($x-y-t$) model are used to interpret some of the full model results. The model results indicate that attention must be paid to details of initialization techniques in spite of the ocean's rapid geostrophic adjustment rates. Toward the end of the model year, a weak anticyclonic eddy is pinched off the Loop Current; probably finer resolution than that offered in this paper is required to increase the intensity of the eddy. Nevertheless, a variety of transient, smaller scale, baroclinic eddies are evident in the calculated circulation patterns. Deficiencies in both the atmo-

spheric and lateral boundary forcing data are identified which should lead to strategies for improved model simulations.

Received February 21, 1984 and in revised form August 19, 1984

Introduction

The Gulf of Mexico is a region of scientific interest due to its intense current systems and large temporal and spatial variability. Moreover, there have been few previous modelling efforts for the Gulf. Those models that do exist do not include thermodynamical processes. The work of Baer et al. (1968) using a four-level quasi-geostrophic model developed by Hamm and Lesser (1968) was the first attempt to produce Gulf circulation patterns. This model, after initialization with data, was used to forecast a four-week period. The results of the forecast showed much temporal variability and large upwelling and downwelling velocities (of the order of the horizontal velocities). While producing interesting results, the model considered only an intermediate region away from surface and bottom influences, and excluded all topographical effects. Paskausky and Reid (1972) developed a barotropic Gulf model that included topography and inertial effects on a β -plane. The results were of limited use since one of the terms in the governing equations (vortex stretching from topographic changes) was inadvertently omitted from the finite difference version. Wert and Reid (1972) constructed a two-layer quasi-geostrophic model that was able to simulate qualitatively the annual cycle of Loop Current intrusion. A barotropic model, a reduced gravity model and, additionally, a two-layer model were used by Hurlburt and Thompson (1980, 1982) to elucidate some of the dynamical processes governing the Loop Current and its attendant eddy shedding. Their investigation showed that temporal variations in the inflow at the Yucatan Straits were not required for realistic shedding cycles and provided useful results for interpreting the effects of resolution and horizontal viscosity.

This article aims to describe and test a numerical three-dimensional circulation model of the Gulf. Realism is stressed in the model presented here in that realistic coastline, bottom topography, atmospheric forcing and oceanic initialization are accommodated. The model includes a free surface, a second moment turbulence closure model which should produce good simulation of the ocean surface layer, and numerical procedures which appear to cope gracefully with large baroclinic and topographic variability. The following sections contain a discussion of the hydrographic and atmospheric surface flux climatologies, data which provide the model with surface forcing, lateral boundary conditions and initialization, and a description of the circulation

calculated by the model which is, whenever possible, compared with oceanographic observations. The model simulation was for a period of one year; it is initialized with climatological temperature and salinity distributions (February 15) and is driven by climatologically derived surface wind stress and heat flux.

Climatology of the Gulf of Mexico

Anticipating the need for model initialization, surface forcing, lateral boundary conditions and data with which to compare model calculations, a climatology of the Gulf of Mexico has been created.

Climatological wind stress, heat flux and effective salt surface flux were determined from data files TDF-11 maintained by the National Climatic Center (NCC); the files consist of over a million Gulf surface ship observations. The raw data were edited and converted with the aid of bulk aerodynamic and radiational exchange formulas to produce monthly estimates of the wind stress statistics, heat flux and mass flux on a 1° square grid. The transfer coefficients in the formulas vary with wind speed and stability in a manner similar to those of Bunker (1976). The stresses and fluxes were then placed on the finer resolution numerical grid by an objective interpolation technique (see appendix by H.J. Herring in Kantha et al., 1981).

The area-averaged wind stresses shown in Figure 1a indicate that while the zonal stress is easterly, weak winter "northers" and summer southerlies are present. The net heat flux of the Gulf shown in Figure 1b (where a positive value implies a net warming of the ocean) shows that the basin loses more heat to the atmosphere during the winter than it gains in the summer time with an annual mean of -48 Wm^{-2} . Annual rates determined by Hastenrath and Lamb (1978), Bunker (1976) as recomputed by Etter (1975, 1983) are somewhat lower, -27 , -21 and -8 Wm^{-2} , respectively. The contribution of the latent heat flux is greater than in the previous estimates and accounts for most of the differences (a reduction of the mass transfer coefficient for evaporation by 25% produces a nearly null, net annual heat flux). The reason for this is not yet clear; it should be noted that all of these heat flux estimates are based on substantially the same data base. The total uncertainty in these calculations was estimated by Hastenrath (1980) to be in the order of $20-30 \text{ Wm}^{-2}$.

The mass budget for the Gulf is shown in Figure

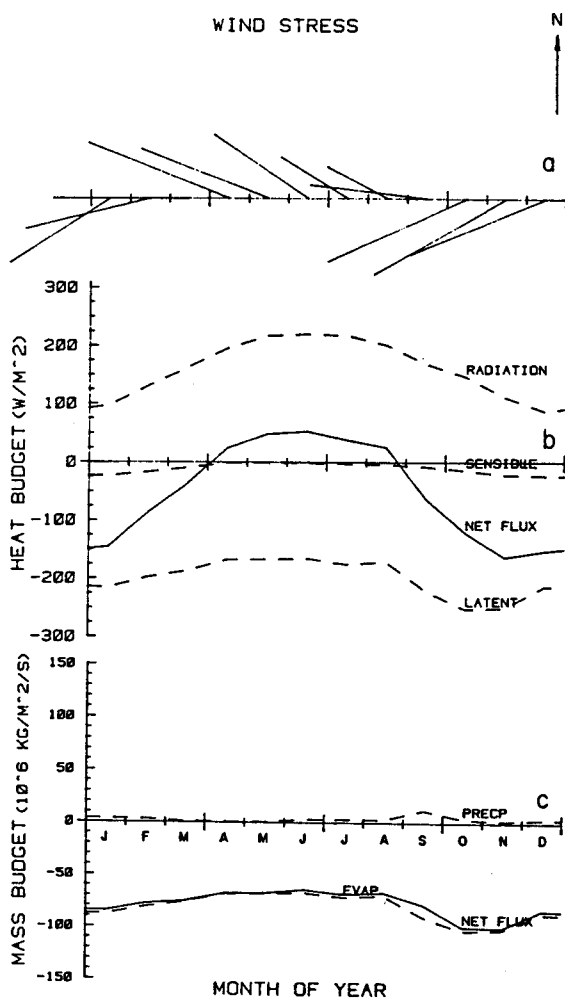


Fig. 1. The annual cycle of Gulf averaged wind stress (a), heat budget (b), and mass budget (c) derived from climatological, atmospheric surface data. Direction of arrow at top right indicates North; its magnitude represents a wind stress of $0.2 \text{ dynes cm}^{-2}$.

1c. The observations of precipitation are much too low. The net mass flux, $-78 \times 10^{-6} \text{ kg m}^{-2} \text{ s}^{-1}$ or equivalently $\sim 250 \text{ cm yr}^{-1}$, is much larger than the estimates of Franceshini (1961), Jacobs (1951), Maul (1979) and Etter (1975). The disparity in these precipitation estimates is not yet understood and further investigation is required. Monthly net heat flux and mean wind stress distributions were calculated from the data and used as boundary conditions for the model; data for every third month is shown in Figures 2 and 3. (Distributions for all months are available from the authors.) These quantities exhibit considerable horizontal structure as well as seasonal variability.

To complement the atmospheric forcing data, the complete set of Gulf temperature and salinity data files maintained by the National Oceanographic Data Center (NODC) were processed. The edited raw data were averaged on a 1° square grid at the standard NODC depth levels. This new data set includes all the data which were archived prior to 1979 and consists of over half a million temperature and salinity observations. The number of observations is about 50% higher than that used by Behringer et al. (1977). Despite this, the quantity of data is still insufficient for forming meaningful monthly Gulf-wide distributions. Seasonally varying distributions are therefore constructed in the upper 1000 m while annual mean values are used between 1000 m and 1500 m; below 1500 m area-averaged, annual mean values are used. This final data set, after being spread onto the model grid points via the objective interpolation technique, is fitted to the vertical levels in the model by linear interpolation. The model uses the data from the first season, averaged January–February–March conditions, and is therefore initialized on February 15. Other seasonal distributions are available against which model simulations can be compared to provide a form of model verification. Figures 4 and 5 show the seasonal temperature and salinity distributions at four levels in the model. Analogous distributions exist at all 15 model levels.

The effect of averaging and interpolating the historical data files is to produce representative but considerably smooth temperature and salinity fields. The thermal manifestation of the Loop Current (Fig. 4) is smoothed considerably when compared to synoptic maps, as is upwelling along the northern and western coasts of Yucatan.

The Circulation Model

The ocean circulation model developed for use in this study is intended to represent ocean physics as realistically as possible. The model is three-dimensional, incorporating a turbulence closure submodel to provide a firm basis for the parameterization of the vertical mixing processes. A complete description of the governing equations and the numerical techniques can be found in Blumberg and Mellor (1983, 1985). For the reader's convenience a brief discussion of the principles and assumptions is presented here.

Two simplifying approximations are used: (i) it is assumed that the weight of the fluid identically balances the pressure (hydrostatic assumption), and (ii) density differences are neglected unless the

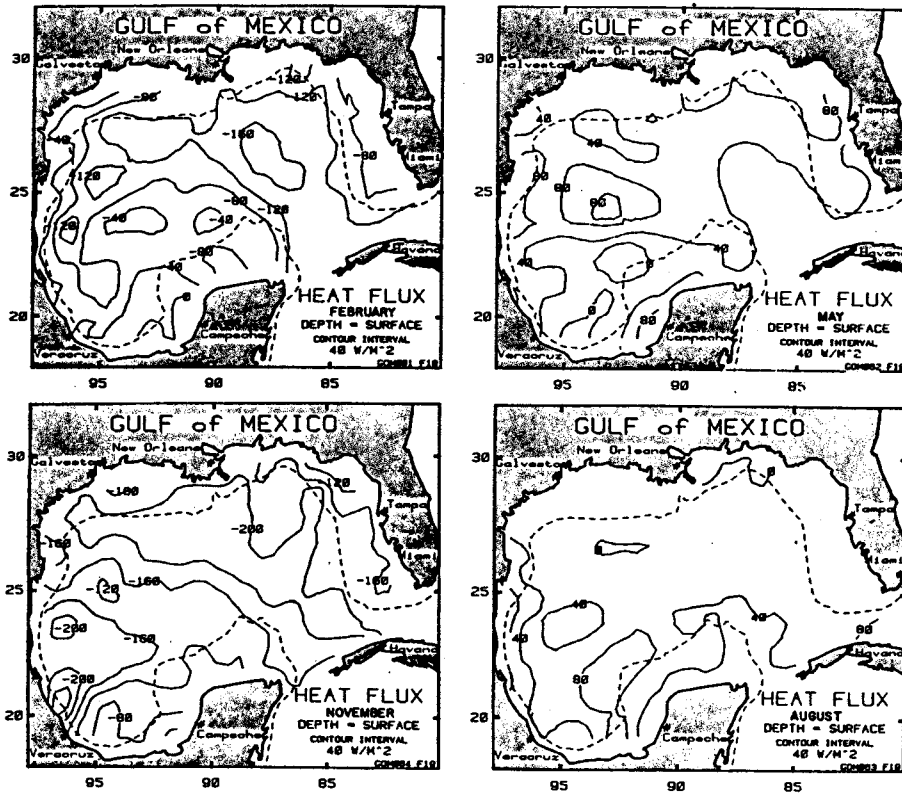


Fig. 2. Monthly mean, observed heat fluxes for February, May, August and November. The time sequence is clockwise.

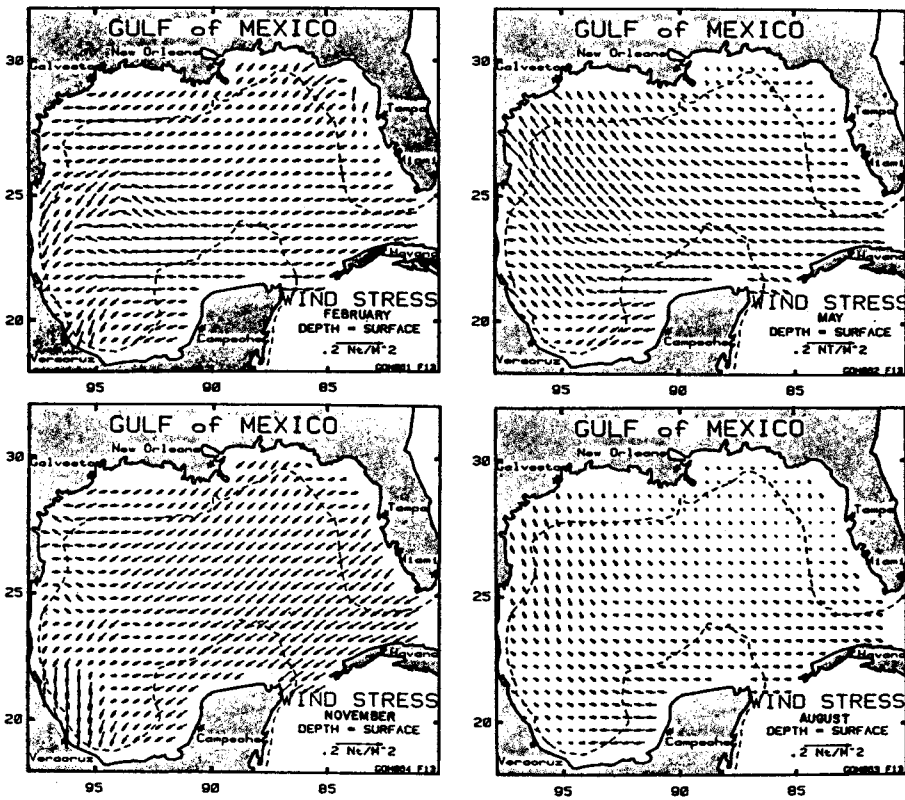


Fig. 3. Monthly mean, observed wind stress vectors for February, May, August and November. The time sequence is clockwise.

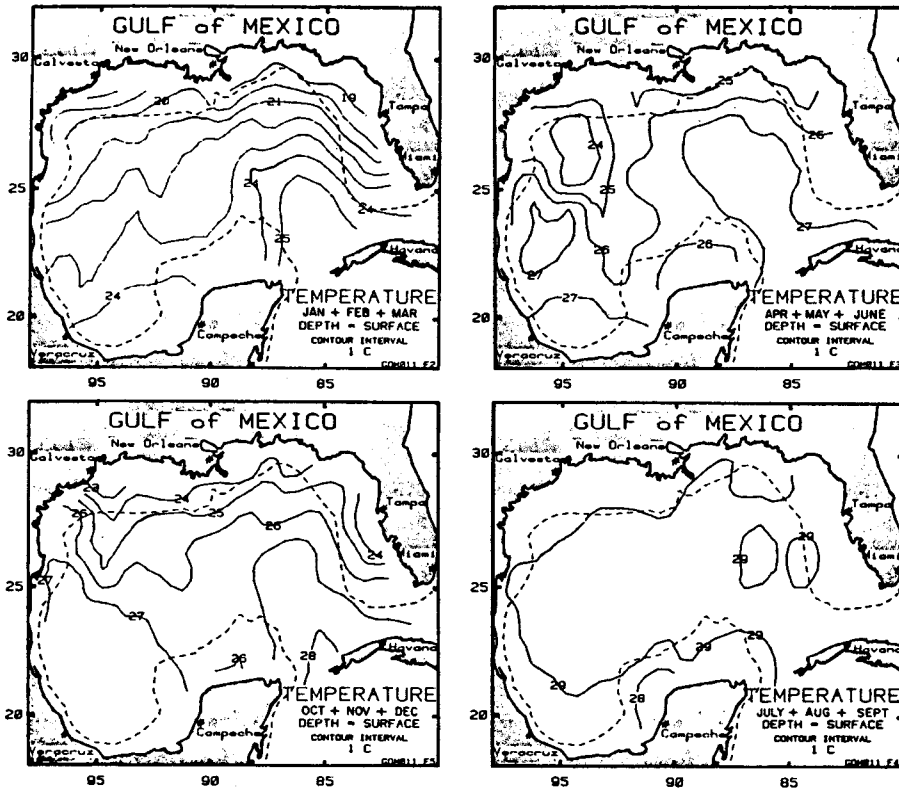


Fig. 4a. Seasonally averaged, observed climatological temperature distributions at the surface. The time sequence is clockwise.

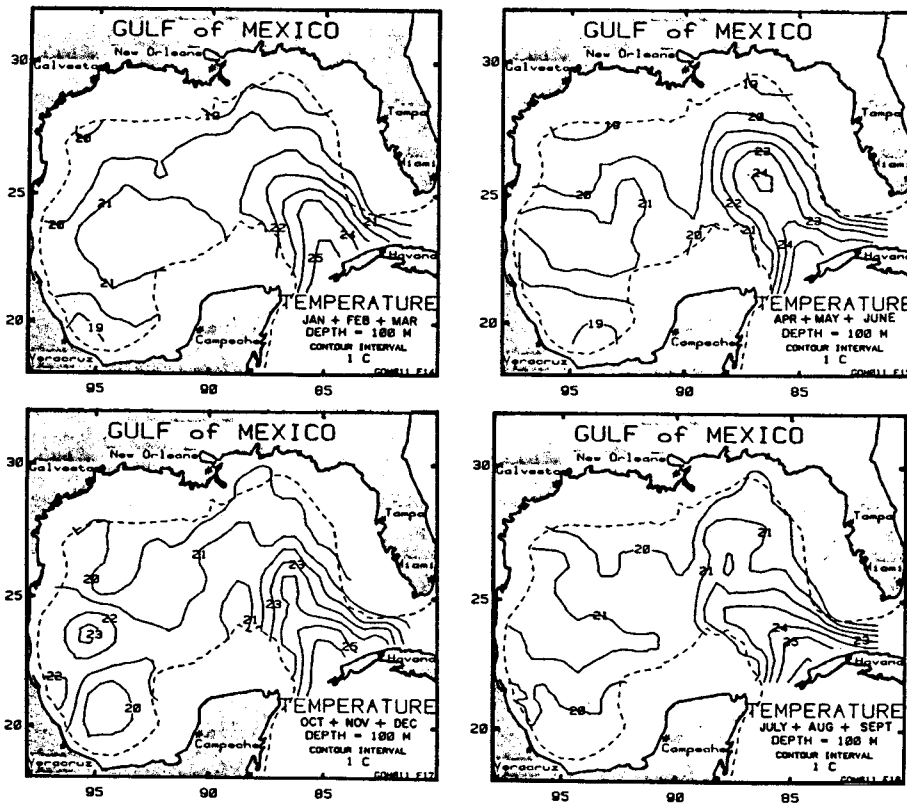


Fig. 4b. Same as Fig. 4a except for the 100-m depth.

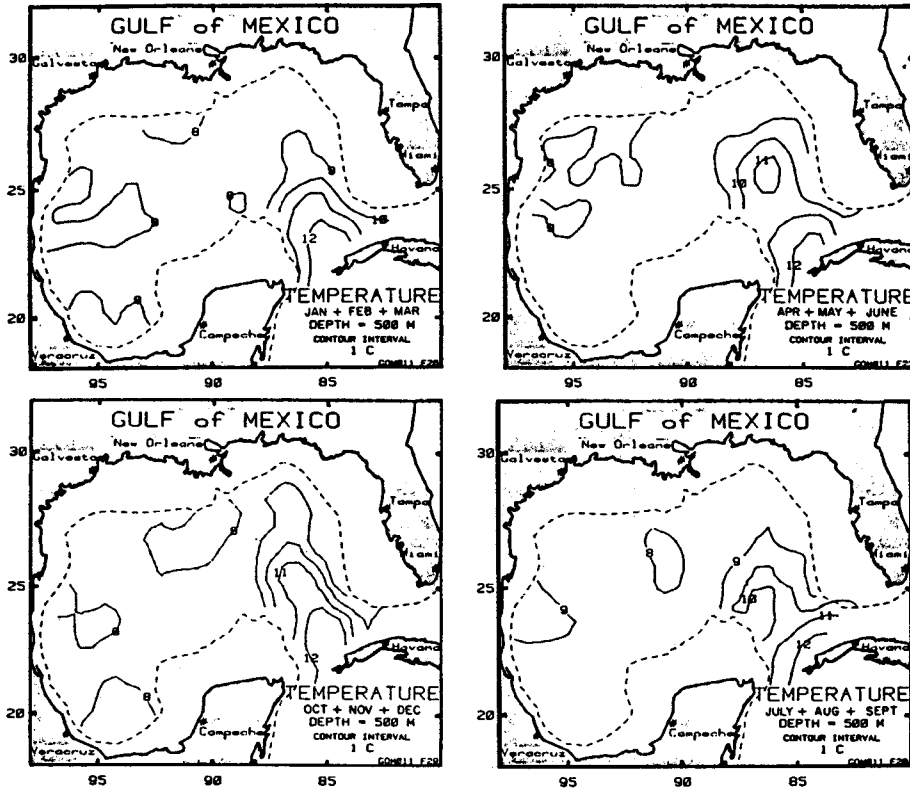


Fig. 4c. Same as Fig. 4a except for the 500-m depth.

differences are multiplied by gravity (Boussinesq approximation). Consider a system of orthogonal Cartesian coordinates with x increasing eastward, y increasing northward and z increasing vertically upwards. The ensemble mean velocities are U , V , W . The free surface is located at $z = \eta(x, y, t)$ and the bottom is at $z = -H(x, y)$.

The continuity equation is

$$\partial U / \partial x + \partial V / \partial y + \partial W / \partial z = 0. \quad (1)$$

The Reynolds momentum equations in conservative form are

$$\begin{aligned} \partial U / \partial t + \partial U^2 / \partial x + \partial UV / \partial y + \partial UW / \partial z - fV \\ = -(1/\rho_0) \partial P / \partial x + \partial / \partial z (K_M \partial U / \partial z) + F_x, \end{aligned} \quad (2)$$

$$\begin{aligned} \partial V / \partial t + \partial UV / \partial x + \partial V^2 / \partial y + \partial VW / \partial z + fU \\ = -(1/\rho_0) \partial P / \partial y + \partial / \partial z (K_M \partial V / \partial z) + F_y, \end{aligned} \quad (3)$$

$$-\rho g = \partial P / \partial z, \quad (4)$$

with ρ_0 , the reference density; ρ , the in situ density; g , the acceleration due to gravity; and P , the pressure.

A latitudinal variation of the Coriolis parameter, f , is introduced by use of the β plane approximation as

$$f = f_0 + \beta y. \quad (5)$$

For the Gulf of Mexico, $f_0 = 6.147 \times 10^{-5} \text{ s}^{-1}$ and $\beta = 2.070 \times 10^{-11} \text{ m}^{-1} \text{ s}^{-1}$ appropriate to a latitude of 25°N .

The pressure at a depth z can be obtained by integrating the vertical component of the equation of motion, equation (4), from z to the free surface, η , and is

$$P(x, y, z, t) = P_{\text{atm}} + g \rho_0 \eta + g \int_z^0 \rho(x, y, z', t) dz'. \quad (6)$$

Henceforth, the atmospheric pressure, P_{atm} is assumed constant.

The equations for the mean of any scalar, Θ_i , may be written

$$\begin{aligned} \partial \Theta_i / \partial t + \partial U \Theta_i / \partial x + \partial V \Theta_i / \partial y + \partial W \Theta_i / \partial z \\ = + \partial / \partial z (K_H \partial \Theta_i / \partial z) + F_{\Theta_i}, \end{aligned} \quad (7)$$

where Θ_i may represent mean potential temperature, Θ , or salinity, S .

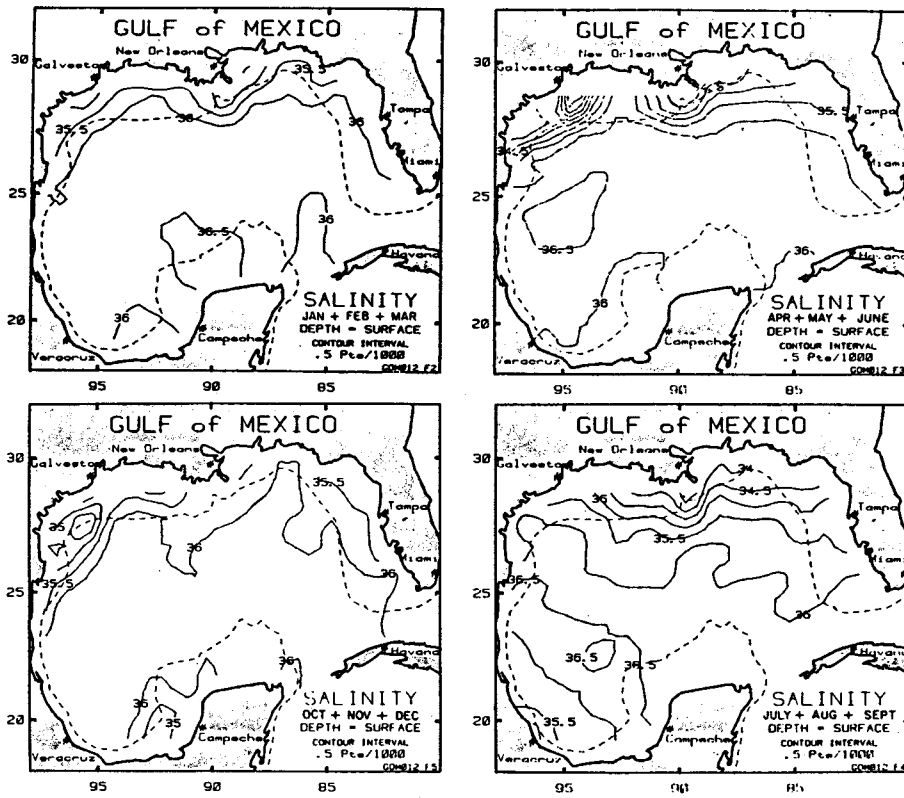


Fig. 5a. Seasonally averaged, observed climatological salinity distributions at the surface. The time sequence is clockwise.

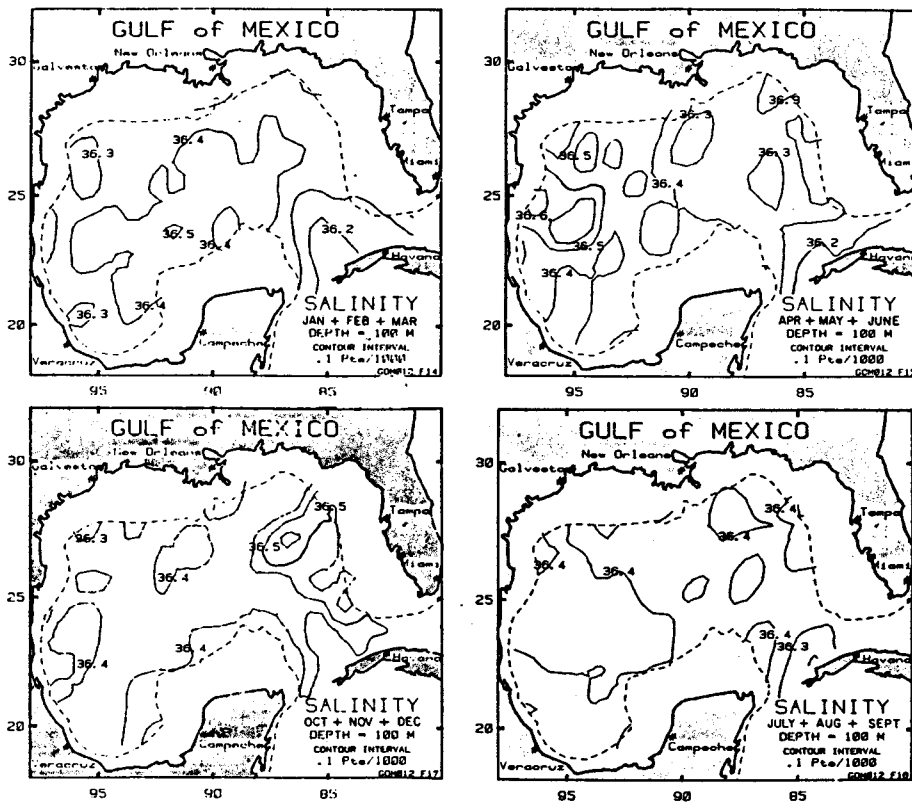


Fig. 5b. Same as Fig. 5a except for the 100-m depth.

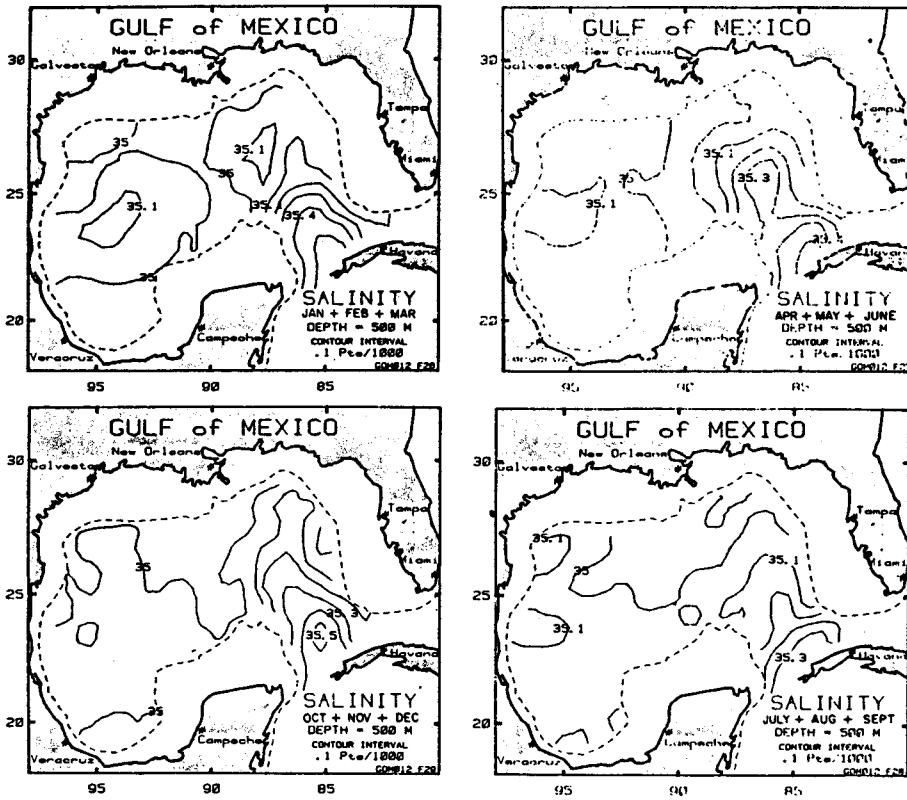


Fig. 5c. Same as Fig. 5a except for the 500-m depth.

Once the temperature and salinity have been computed, the density is represented (see Fofonoff, 1962) as

$$\rho = \rho_{\theta}(\Theta, S), \quad (8)$$

where ρ_{θ} is the potential density.

The vertical mixing coefficients in Eqs. (2), (3) and (7) are obtained by appealing to a second order turbulence closure scheme (Mellor & Yamada, 1982). While the details of the closure model are rather involved, it is possible to reduce the prescription of the mixing coefficients to a form functionally dependent upon $\partial U/\partial z$, $\partial V/\partial z$, $g\rho_0^{-1}\partial\rho/\partial z$, q and l . Furthermore, the closure model provides a set of differential equations which characterizes both the turbulence kinetic energy, $q^2/2$, and the turbulence macroscale, l .

The terms F_x , F_y , and F_{Θ_i} found in Eqs. (2), (3) and (7) represent horizontal viscosity and diffusion and are written as

$$F_x = A_M(2\partial^2 U/\partial x^2 + \partial/\partial y(\partial U/\partial y + \partial V/\partial x)), \quad (9a)$$

$$F_y = A_M(2\partial^2 V/\partial y^2 + \partial/\partial x(\partial U/\partial y + \partial V/\partial x)), \quad (9b)$$

and

$$F_{\Theta_i} = A_H \nabla^2 \Theta_i, \quad (10a)$$

where ∇^2 is the Laplacian operator. These horizontal diffusive terms are meant to parameterize subgrid scale processes. However, in practice the horizontal diffusivities are usually required to damp small scale computational noise. The form of F_x and F_y used here is such that they are invariant to coordinate rotation.

The boundary conditions at the free surface, $z = \eta(x, y)$, are:

$$\rho_0 K_M (\partial U/\partial z, \partial V/\partial z) \sim (\tau_{0x}, \tau_{0y}) \text{ as } z \rightarrow \eta, \quad (11a)$$

$$\rho_0 C_P K_H (\partial \Theta/\partial z, \partial S/\partial z) \sim (\dot{H}, \dot{S}) \text{ as } z \rightarrow \eta, \quad (11b)$$

$$q^2 = B_1 u_r^2, \quad z = \eta, \quad (11c)$$

$$q^2 l = 0, \quad z = \eta, \quad (11d)$$

$$W = U\partial\eta/\partial x + V\partial\eta/\partial y + \partial\eta/\partial t, \quad z = \eta, \quad (11e)$$

where (τ_{0x}, τ_{0y}) is the surface wind stress vector, \dot{H} is the net ocean heat flux, and $\dot{S} \equiv S(0)(\bar{E} - \bar{P})/\rho_0$

where $(\bar{E} - \bar{P})$ is the net evaporation–precipitation fresh water surface mass flux rate. In Eq. (11c), $u_\tau = |\tau_0/\rho_0|^{1/2}$ is the friction velocity and B_1 is one of the empirical constants in the turbulent closure relations. In the present version of the model the boundary conditions are linearized about $z = 0$. This introduces a small error as it neglects the storage of mass and Θ_i in the region between $z = 0$ and $z = \eta$.

At the bottom, $z = -H(x, y)$, zero vertical flux for Θ and S are stipulated, that is,

$$K_H(\partial\Theta/\partial z, \partial S/\partial z) = 0, \quad z = -H. \quad (12a)$$

At the bottom the macroscale, l , is zero, thus

$$q^2 l = 0, \quad z = -H \quad (12b)$$

and

$$q^2 = B_1 u_\tau^2, \quad z = -H. \quad (12c)$$

Now, u_τ is the friction velocity associated with the bottom frictional stress. Also at the bottom,

$$W = -U\partial H/\partial x - V\partial H/\partial y. \quad (12d)$$

The horizontal velocities are not set to zero at the bottom; instead, they are subjected to a bottom stress at $z = -H$ of the form

$$K_M \partial/\partial z (U, V) \sim (\tau_{Hx}, \tau_{Hy}) = k(U, V) |U|, \quad (13)$$

where (τ_{Hx}, τ_{Hy}) is the bottom stress vector and $k = 0.0025$.

The presence of lateral boundaries imposes additional constraints on the governing equations. At “closed” land–water interfaces a no-slip condition is invoked on the velocity field. Another condition is that there are no diffuse fluxes of any property into or out of these interfaces. These boundary conditions insure proper conservation properties. The “open” seaward boundary conditions are more difficult. Basically, the problem is to parameterize correctly the environment exterior to the relevant domain. With this in mind, one can identify two types of open boundaries, inflow and outflow. Temperature and salinity are prescribed from data at an inflowing boundary whereas at outflow boundaries $\partial\Theta/\partial t + U_n \partial\Theta/\partial n = 0$ is solved where the subscript n is the coordinate normal to the boundary. Turbulence kinetic energy and the macroscale quantity ($q^2 l$) are calculated with sufficient accuracy at the boundaries by neglecting the advection in comparison with other terms in their respective equations.

The vertical shear of the normal component of velocity is determined from geostrophic balance at

the open boundaries. Absolute velocities can be obtained by assuming a level of no motion at the bottom and this is, of course, tantamount to a knowledge of the sea surface slope. Generally, the net total transport of an “open” region computed in this way will not balance so that the region will either fill or empty as time progresses. Therefore, the normal velocity distribution must be corrected to ensure balance. Details are discussed in the next section. A free-slip condition is specified for the tangential component of velocity at the open boundaries.

Numerical Methodology and Model Parameters

The governing equations together with their boundary conditions are solved by finite difference techniques with a staggered “C” grid (Arakawa & Lamb, 1977). The staggered arrangement uses U at points to the east and west of the point where η and H are defined and V at points to the north and south of the η and H points. The horizontal grid increments are constants, while the vertical increment Δz varies in thickness to accommodate more resolution near the surface. The time differencing is the conventional leap-frog technique. However, the scheme is quasi-implicit in that vertical diffusion is evaluated at the forward time level. Thus, small vertical spacing is permissible near the surface without the need to reduce the time increment or restrict the magnitude of the mixing coefficients. A mode splitting technique (Simons, 1974) has been implemented for computational efficiency. It should be noted that the finite difference equations conserve energy, Θ_i , mass and momentum. Also they are second order accurate in space and time when dissipation is neglected. Details of the finite difference equations and computer programming techniques are presented in Blumberg and Mellor (1983, 1985).

The Gulf of Mexico was schematized onto a computational grid with a horizontal resolution of $\frac{1}{2}^\circ \times \frac{1}{2}^\circ$ (50 km \times 55 km) representing a 34×24 lattice of points as illustrated in Figure 6. All depths less than 30 m were considered to be land areas. The bottom topography used in the model is also shown in Figure 6. The topographic data was digitized from Nautical Chart 411 available from the National Ocean Survey. Since the model has 16 levels in the vertical, the actual topographic data was fitted to the nearest model level causing a slight distortion of the bottom shape. The distribution of grid points in the vertical is given in Table 1. The quantity, z , corresponds to the depth at which horizontal velocity, θ_i and density

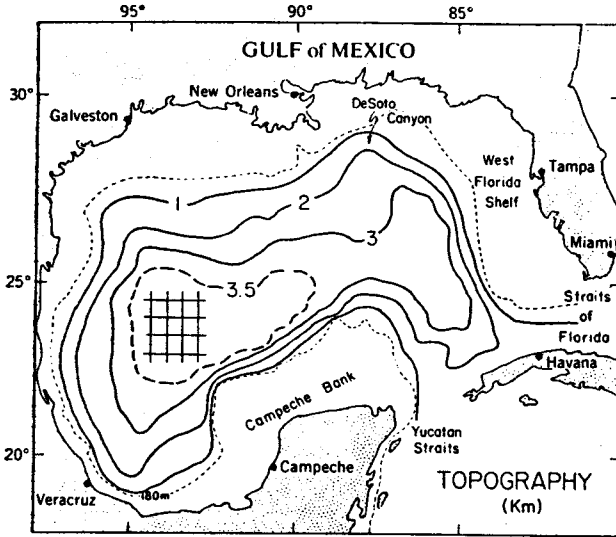


Fig. 6. The bottom topography used in the Gulf of Mexico circulation model. The "checker board" pattern is a detailed view of the horizontal grid schematization with the spacing being 50 km X 55 km. Geographical features referred to in the text are labeled.

are located, while z' refers to the depths at which the turbulence quantities and the vertical velocity are defined. The fine vertical resolution near the surface, along with the logarithmic grid spacing, ensure that the surface layers will be resolved well as demonstrated by Blumberg and Mellor (1983). The external mode time step is 36 s whereas the internal time step is 100 times larger, or 1 h.

TABLE 1. The Vertical Distribution of Grid Points. The Quantity z' Refers to the Depths at which the Turbulence Quantities and the Vertical Velocity are Located, while z Corresponds to the Depth at which Horizontal Velocity, Θ , and Density are Defined

Level	z' (m)	z (m)
1	0	1
2	2	3
3	4	6
4	8	12
5	16	24
6	32	48
7	64	96
8	128	192
9	256	384
10	512	768
11	1024	1280
12	1536	1792
13	2048	2304
14	2560	2816
15	3072	3328
16	3584	

The numerical solutions are also dependent on the horizontal viscosity, A_M , and the horizontal diffusivity, A_H . The values used in this study are $A_M = 4 \times 10^3 \text{ m}^2 \text{ s}^{-1}$ and $A_H = 2 \times 10^3 \text{ m}^2 \text{ s}^{-1}$. Sturges and Blaha (1976) have postulated the existence of a western boundary current in the Gulf, in which case the boundary current width, according to Munk (1950), is of order $2(A_M/\beta)^{1/3} \cong 150 \text{ km}$ and is therefore not quite resolved. Short term, preliminary numerical tests with lower A_M and A_H indicate that a reduction by a factor of four is possible with the $1/2^\circ$ resolution and this numerical scheme. Future simulations will use lower values. The only other adjustable physical parameter is the background vertical mixing coefficient. The results of a sensitivity study by Blumberg and Mellor (1979) on the seasonal variability as simulated by an area-averaged numerical model indicate that this coefficient should be $1 \times 10^{-4} \text{ m}^2 \text{ s}^{-1}$. This value is on the order of 100 times smaller than the model-generated values in the upper mixed layer.

The choice of wind stress statistics is governed and complicated somewhat by the fact that surface-layer mixing depends synoptically on $\tau_0 \equiv |\tau_0|$ where τ_0 is the surface wind stress vector. The required climatological average should be $\bar{\tau}_0 \equiv |\bar{\tau}_0|$. On the other hand, Ekman transports depend on τ_x and τ_y . Their climatological average and the resultant general circulation require $\bar{\tau}_x$ and $\bar{\tau}_y$. The data set when averaged over all months and over the whole Gulf yields $\bar{\tau}_0 = 0.6 \text{ dynes/cm}^2$, $\bar{\tau}_x = -0.3 \text{ dynes/cm}^2$ and $\bar{\tau}_y = -0.01 \text{ dynes/cm}^2$. Clearly, climatological averages of τ_x and τ_y will underestimate the stress needed for proper mixing. To satisfy both the surface mixing and general circulation requirements, a simple two-component wind model has been devised to drive the Gulf circulation model (see Blumberg and Mellor, 1983, for graphical representation).

$$\tau_x = \tau_0(x,y) [(1 + A \cos \omega_1 t) \cos(\omega_1 t + \phi) + 0.1 \cos \omega_2 t], \quad (14)$$

$$\tau_y = -\tau_0(x,y) [(1 + A \cos \omega_1 t) \sin(\omega_1 t + \phi) - 0.1 \sin \omega_2 t], \quad (15)$$

where $\omega_1 = 2\pi T_1^{-1}$ and $\omega_2 = 2\pi T_2^{-1}$. The value $T_1 =$ four days is prescribed to represent roughly the passage of tropical and subtropical cyclones and $T_2 =$ one day as a token representation of the diurnal cycle. The parameters τ_0 and ϕ are slowly varying

functions of time interpolated from the monthly climatological averages and are obtained according to $\tau_0 = 2(\bar{\tau}_x^2 + \bar{\tau}_y^2)^{1/2}$ and $\phi = \tan^{-1}(-\bar{\tau}_y/\bar{\tau}_x)$. The data has also been used to determine that A is very close to unity; therefore, $A = 1$ is specified in the model. The wind stresses specified by this wind model, of course, contain the means shown in Figure 3, but also closely approximates the observed monthly average of $|\bar{\tau}_0|$. Nevertheless this wind model may still be too simplistic in view of the work of Klein (1980) who has demonstrated that averaging wind fields tends to reduce mixed-layer deepening.

The original intent of the model development was to study the environmental impact of OTEC powerplants which can change the sea surface temperature. Therefore, to account for this physical process, feedback has been added to the heat flux boundary condition so that

$$\dot{H} = \dot{H}_{\text{data}} + \gamma(T_{\text{data}} - T) \quad (16)$$

where \dot{H}_{data} and T_{data} are the data-determined heat flux and surface temperature, respectively, and T is the model-predicted surface temperature. The data reduction effort has also been used to determine that $\gamma = 50 \text{ W/m}^2\text{°C}$. This particular mechanism assumes that the heat flux change is only dependent upon the difference between the predicted and data-determined surface temperatures. (The value of $\gamma = 50 \text{ W/cm}^2\text{°C}$ was actually determined by adding one degree to the observed sea surface temperature and computing the incremental change in \dot{H} . The spatial and temporal variability of γ was quite small and justified use of a constant value. The procedure does not include the secondary feedback due to the atmospheric response to the sea surface temperature disturbance.) In those simulations without OTEC plants, Eq. (16) can be thought of as a way to drive a model using both the imposed heat flux and surface temperature.

The initial velocity fields are simply set to zero. Diagnostic numerical experiments conducted in the initial phases of this research effort indicate that the energetics of the velocity field are steady after about seven days. This is in accord with the results of Holland and Hirschman (1972) that show a 20-day adjustment period of a much larger domain, the Atlantic Ocean, and with the 10-day spin-up time of Blumberg and Mellor (1983) for a Gulf-sized South Atlantic Bight domain. During model development the start-up shock produced by setting the initial velocity fields to zero is most useful as computer

programming deficiencies are quickly revealed. However, the geostrophic adjustment processes rapidly lead to displacements of the initially dynamically unbalanced isopycnals (isotherms and isohalines). The displaced distributions essentially become the new initial conditions for the simulation. Undoubtedly a very smooth start of the model should, in future runs, perhaps be achieved by some form of dynamical initialization (Miyakoda et al., 1978); for ocean applications geostrophic balance may be a satisfactory initial state.

The oceanic boundary conditions in the Yucatan Straits and Straits of Florida can also be obtained by use of the edited NODC data set. Both of these regions were divided into four horizontal $\frac{1}{2}^\circ$ square boxes in an attempt to avoid some of the smoothing which occurred with the Gulf-wide seasonal data sets. The data was then sorted into cross sections as a function of season and depth. Velocity profiles were then inferred from geostrophy, assuming a level of no motion at the bottom. The total transports associated with the profiles were quite variable and there were large differences between inflow and outflow at particular seasons. (For the four seasons, values of 29.7, 31.9, 32.1 and 34.4 Sv were obtained at the Yucatan Straits. However, at the Straits of Florida the transports were 35.6, 14.0, 23.7 and 34.8 Sv (1 Sv $\equiv 10^6 \text{ m}^3 \text{ s}^{-1}$)).

Augmented by an approximate knowledge of the total transport flowing into and out of the Gulf of Mexico, Niiler and Richardson (1973), and Molinari et al. (1978), the temperature and salinity profiles at the two Straits were adjusted until a transport of $30 \times 10^6 \text{ m}^3 \text{ s}^{-1}$ was obtained for each season. This adjustment process, actually an "unsmoothing" of the data, was accomplished by an interactive procedure whereby the tilting of isotherms and isohalines at a particular cross section were proportionately adjusted until geostrophically obtained velocities produced a net transport of $30 \times 10^6 \text{ m}^3 \text{ s}^{-1}$.

The procedure for prescribing boundary conditions is quite straightforward. An atmospheric data library consisting of the monthly mean values of the surface stress and the monthly heat flux distributions at all surface grid points is created. The seasonally varying velocity profiles and temperature and salinity distributions (inflow only) at the two straits are stored in a similarly constructed oceanic data library. As the calculation proceeds, the proper data is selected from the libraries and inserted into the Gulf model by means of linear interpolation.

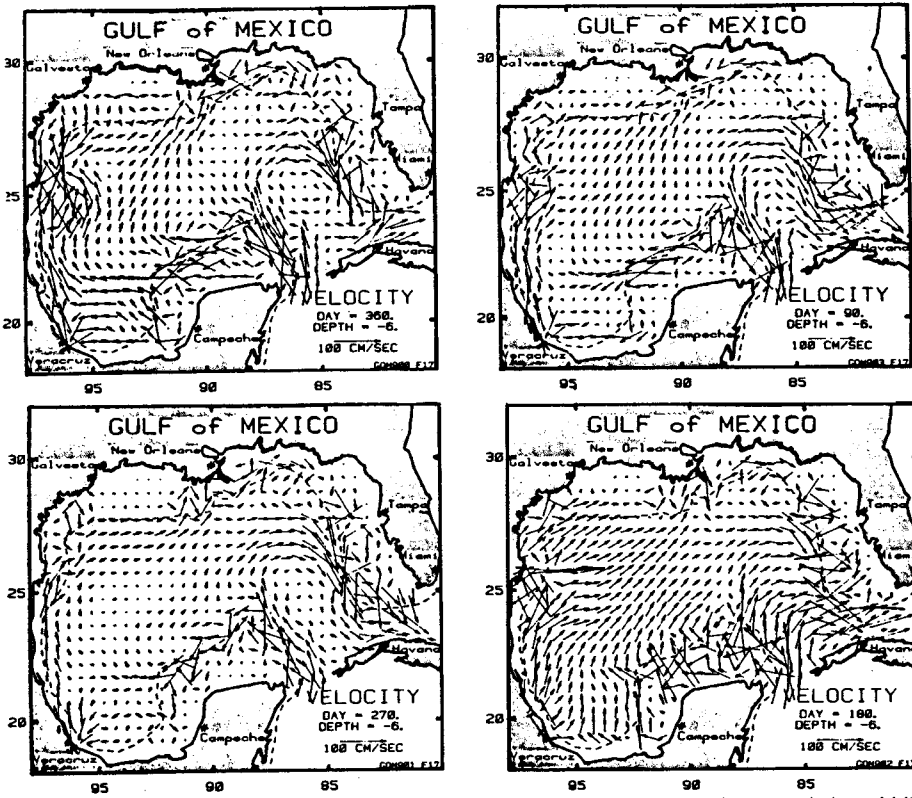


Fig. 7a. Calculated velocity at 6 m below the surface. The sequence is clockwise and the middle day of the months February, May, August and November are shown.

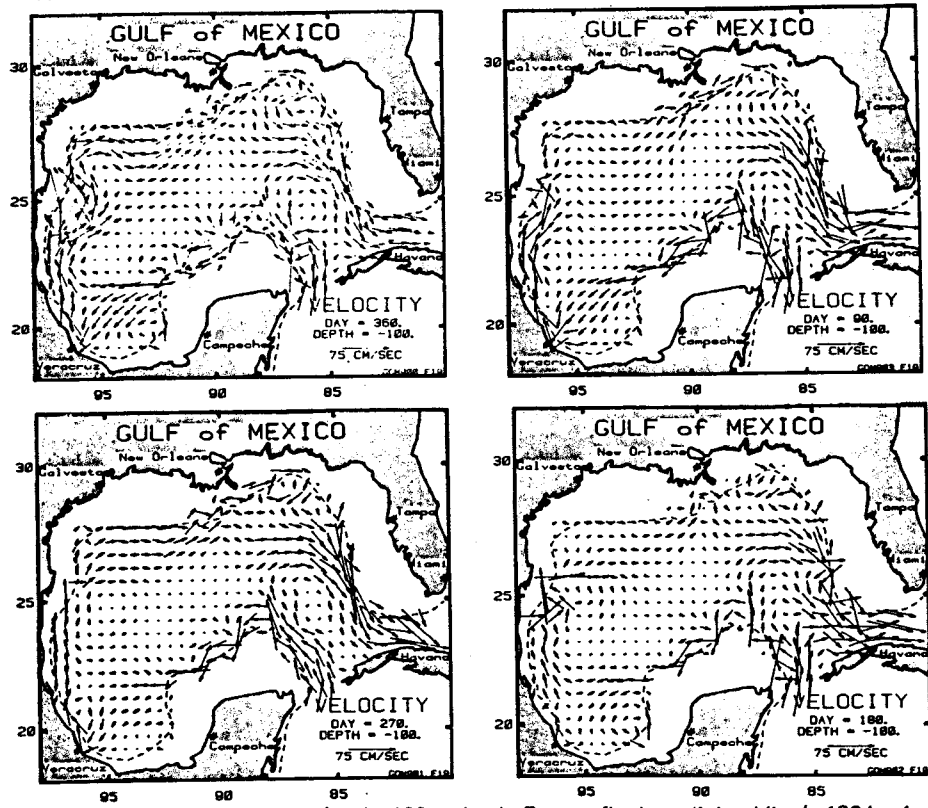


Fig. 7b. Same as Fig. 7a except for the 100-m depth. Four to five baroclinic eddies (~180 km in diam) can be identified in each picture.

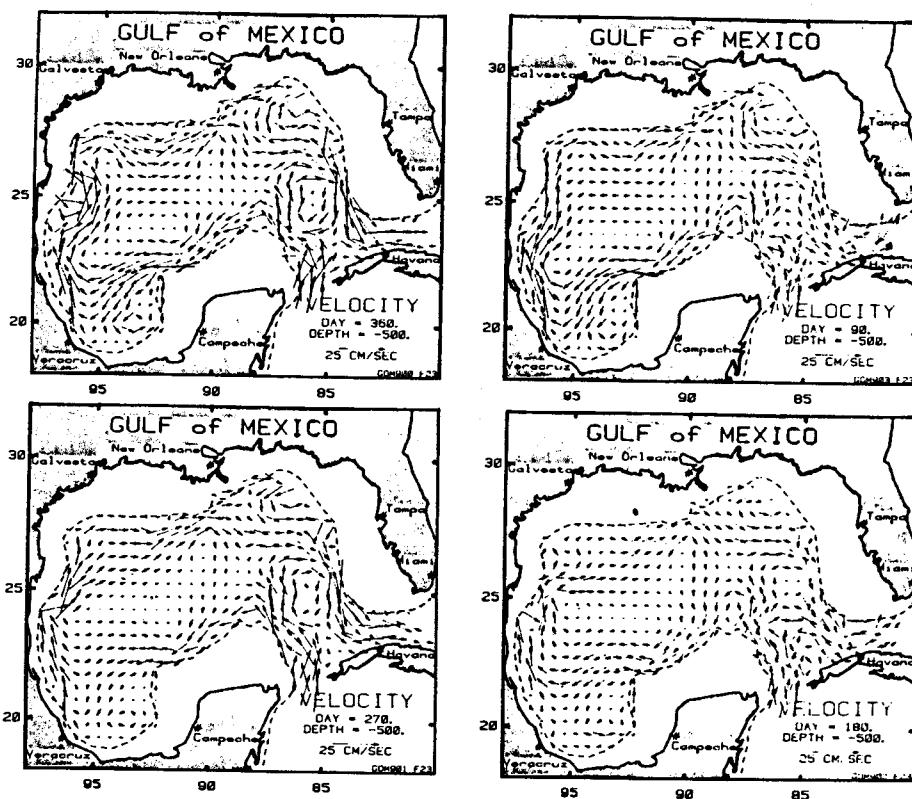


Fig. 7c. Same as Fig. 7a except for the 500-m depth.

Simulated Gulf of Mexico Climatological Circulation

The simulated climatological circulation in the Gulf of Mexico is produced by a year-long integration of the numerical model. The model year consists of 360 days, beginning February 15, using climatological season 1 to initialize the temperature and salinity fields. It was assumed that this date approximated the three-month seasonal average. The results of the simulation are presented in the form of horizontally distributed as well as area-averaged values. The selected depths are chosen to coincide with standard oceanographic levels and are interpolated from the model levels.

The model produces synoptic output and even though driven by climatological boundary conditions (but note again, Eqs. (14) and (15)) cannot be compared directly with climatological hydrography which is nearly all that is available. Nevertheless, the model simulations can be assessed by their general consistency with observations. In particular, the ability of the model to produce a similar variability, intensity, position and extent of the observed major current systems will be apparent. Another effective

way of validating the model predictions is to make sure that they reproduce the essential features of the seasonal thermal variability of the upper layers. The observed large-scale features of the circulation of the Gulf of Mexico and the efforts towards understanding them have been discussed by Molinari et al. (1978), Elliott (1982), Nowlin and McLellan (1967), Sturges and Blaha (1976) and Leipper (1970), among others.

Time sequences of the calculated velocity patterns at 6 m, 100 m, and 500 m depth are illustrated in Figure 7. So that the seasons correspond to the graphical arrangement of the climatological data to be discussed later, the last computational day is located in the upper left hand corner of these figures. The most overt features of the circulation are the persistence of the Loop Current and of an anticyclonic gyre in the western portion of the Gulf. These features are evident at all depths away from the surface layers where wind-induced Ekman currents prevail.

No large amplitude anticyclonic eddies have separated from the Loop Current (Ichiye, 1962; Reid, 1972; Elliott, 1982). As discussed below, only a weak

eddy shedding event has occurred during the model year run. According to the study by Hurlburt and Thompson (1980, 1982), horizontal viscosity needs to be decreased by a factor of about four and the horizontal resolution decreased by a factor of two before eddy shedding instabilities occur. However, there may not be a one-to-one correspondence between their simple models with neither thermodynamics nor atmospheric forcing and the present model. They also demonstrated that while a large value of the horizontal viscosity will prevent discrete eddies from shedding, a large value is an effective way to parameterize the mean over many eddy cycles. The model results presented here do exhibit seasonal variability. The Loop seems to penetrate further northwestwards into the Gulf during the late fall and winter than it does at other times. The August currents at 500 m, for example, show that the Loop has receded to the south.

A number of small eddies, in spite of the 50 km resolution, can be identified in the model results of Figure 7. One can see approximately four to five eddies of ~ 180 km diam (about 4 Rossby radii) in any of the illustrations shown in Figure 7b. For the most part the eddies extend to approx. 500 m depth. Some of the eddies are permanent (over the DeSoto Canyon for example) but most form and dissipate in a matter of a few months.

The near-surface currents are large as they are subject to strong wind effects. The velocities in the Loop are organized and comparable to those observed by Hubertz et al. (1972). Surface currents diminishing in speed as they approach the region of maximum loop curvature have been observed in the Gulf by Kirwan et al. (1975). The observational and theoretical work of Chew (1974) also demonstrated this point. The surface manifestation of a cyclonic eddy near 25°N , 96.5°W , south of Brownsville, Texas, is evident in February and August. This cyclonic feature, accompanied by intense upwelling, is quite similar to the one observed by Merrell and Morrison (1981) and Brooks and Legeckis (1982). The simulated eddy might have migrated to the western Gulf from the Loop Current region as suggested by Merrell and Morrison (1981). On the other hand, it also appears reminiscent of a locally forced circulation, analogous to the one arising from the "Charleston Bump" in the South Atlantic Bight (Brooks & Bane, 1978). In the shallow waters along both the Texas coast and the Campeche Bank there seems to be a wind driven westward flow, while the central portion of the Gulf

exhibits a surface flow to the north and the northeast in agreement with Ekman dynamics for these particular winds.

The circulation in the central Gulf indicates a year-round westward flow north of the Campeche Bank at all depths. This current seems to approach the Mexican coast at 22° – 23°N during some months (e.g. August) and at other times turns southwest flowing over the Campeche Canyon before approaching the coast. As this current approaches the coast and turns north, it flows along the western boundary to about 20°N where it turns east and begins a re-circulation gyre. This current system is similar to that proposed by Sturges and Blaha (1976). They conclude that the maximum flow occurs in December and this is in agreement with model results. Since there have been no rings pinched off the Loop Current in the model year-long simulation, the western basin is probably driven by the wind stress curl as the gyre persists throughout the prediction period.

A smaller scale, permanent cyclonic eddy in the vicinity of the DeSoto Canyon near 28.5°N and 87.5°W is apparent at all depths in the predicted results. These results compare well with observational evidence presented by Molinari et al. (1978). In both situations (data and model predictions) the eddy extends south as a trough across the narrowest portion of the deep basin and appears in all seasons.

No consistent circulation emerges from the model results for the West Florida Shelf area. A strong, rather steady flow exists flowing southward along the Shelf break, but the dynamics on the Shelf seem to be a result of the local wind. The flows are highly variable with May conditions producing the weakest overall patterns. The work of Jones (1973) corroborates these predictions.

The deep currents (not shown) in the Gulf weaken considerably as the bottom is approached. At 1000 m depth the currents are about 5 – 10 cm s^{-1} while at 2800 m the speeds are less than half of these. In all instances the deep flow consists of anticyclonic gyres around the two rather deep, almost independent basins.

The temporal and spatial variation of the height of the free surface in the Gulf as predicted by the model is shown in Figure 8. The Loop Current appears as a bundle of height contours with maximum differences of perhaps 45 cm across it. The largest gradients occur in the May and August distributions with smaller values of 30 cm in February and November.

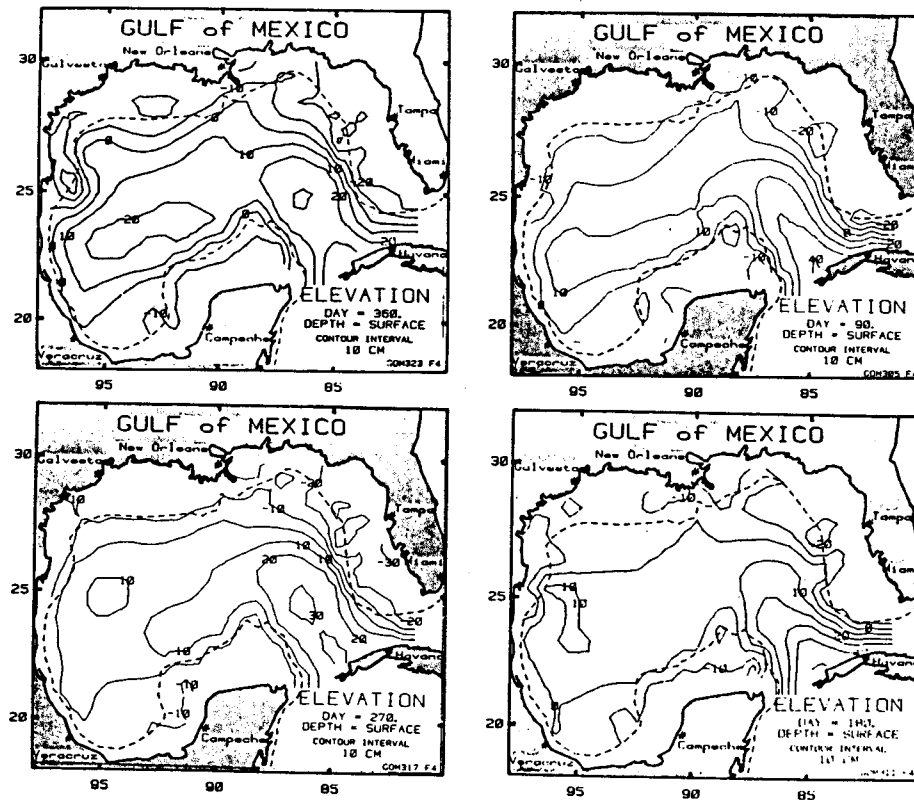


Fig. 8. Calculated surface elevations. The sequence is clockwise and the middle day of the months February, May, August and November are shown.

The dynamic topography of the sea surface with respect to a 1000 m reference level computed by Molinari et al. (1978) shows similar characteristics. That the transports are largest in February and November when the elevation gradients are weakest implies that the wind has a considerable influence at these times. Finally, the February distribution shows most clearly the high (anticyclone) and low (cyclone) pressure distributions in the western basin.

The time sequence of calculated surface elevations shown in Figure 8 indicates that a weak shedding event has occurred. By following both the 10- and 20-cm isoheights throughout the course of the year one finds that there seems to be an eddy (20 cm contour) embedded within the westward bending of the Loop Current (10 cm contour). This type of weak shedding was duplicated with a two-dimensional ($x-y-t$) reduced gravity model (see Hurlburt and Thompson (1980) for the governing equations) using the same parameters and resolution as the full three-dimensional model. When the horizontal grid spacing was decreased to 25 km along with a 10-fold decrease in the horizontal diffusivity, strong eddies were shed

on a periodic basis. It appears that for more intense eddy shedding the 50 km resolution must be improved; probably a grid spacing of 25 km is the largest that will support proper shedding dynamics.

The predicted temperature and salinity distribution near the surface and at 100 m and 500 m below it are shown in Figures 9 and 10. As mentioned previously, the observed climatological temperature and salinity analysis procedures introduce smoothing of observed gradients. The model, on the other hand, predicts fields with greater spatial and temporal variability. The near-surface temperature fields show small scale shelf intrusions and fronts. The horizontal structure of the surface salinity fields has practically vanished due to neglect of river inflow and surface mass flux. Both of these deficiencies can be remedied by appropriate changes in boundary condition definition. Below the surface layers the Loop structure in the data and model results are quite similar with respect to areal extent and tilt angle.

The hydrography associated with cyclonic eddy south of Brownsville is manifest in Figures 9 and 10. Intense upwelling of the isotherms and isohalines is

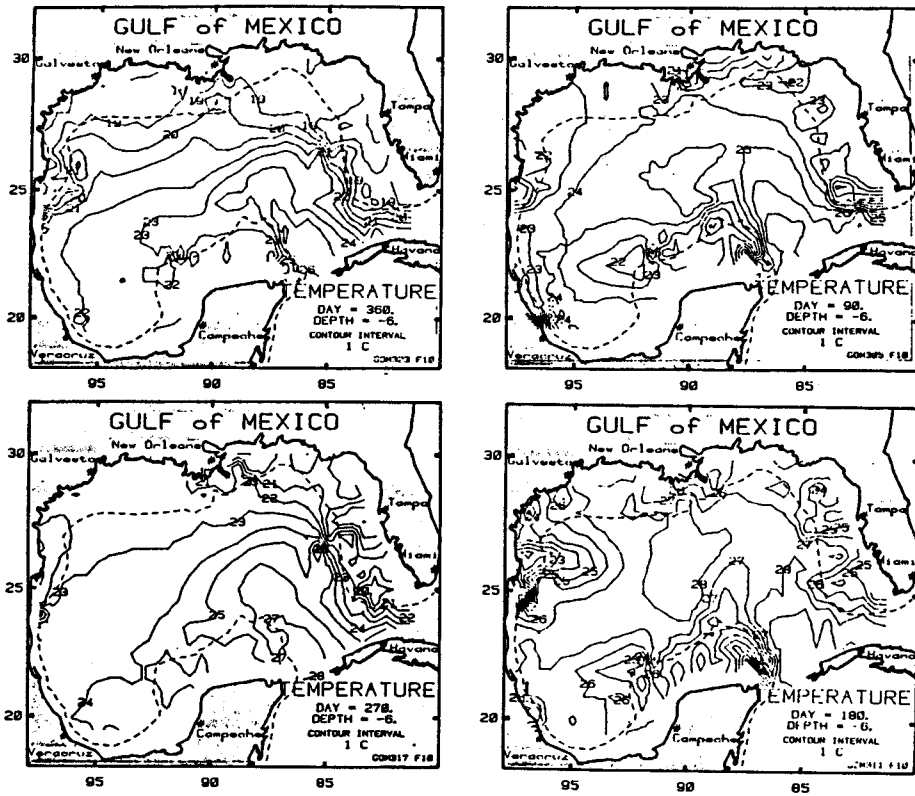


Fig. 9a. Calculated temperature distributions at 6 m below the surface. The sequence is clockwise and the middle day of the months May, August and November are shown. The initial condition on February 15 is that of Fig. 4 for January, February and March. The field shown here for February (15th) is the final calculated field.

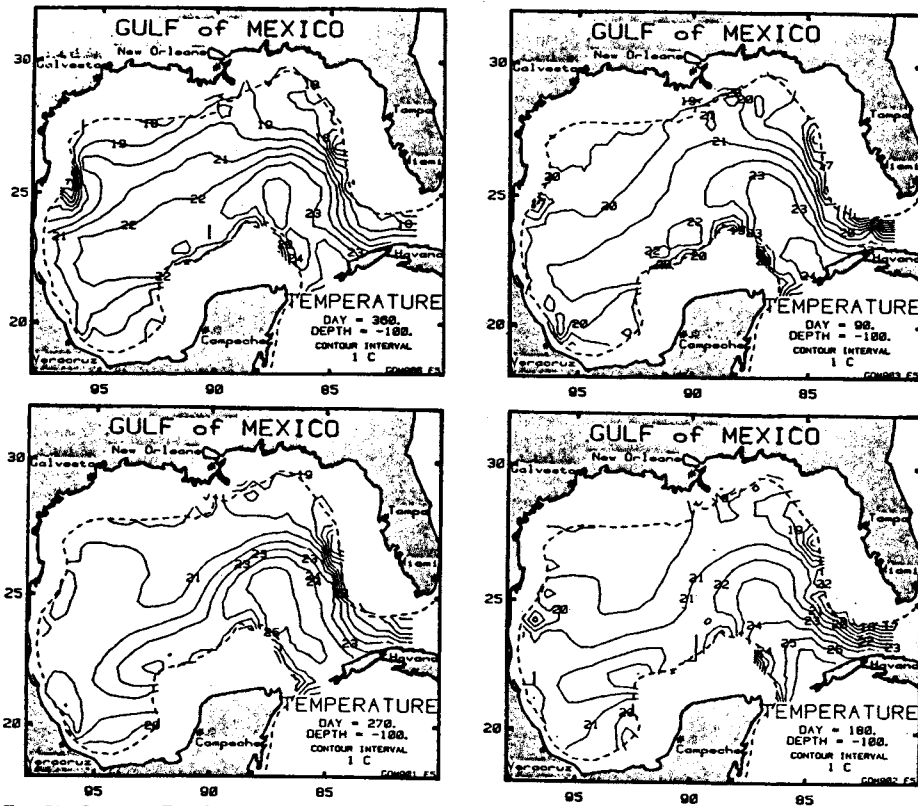


Fig. 9b. Same as Fig. 9a but for the 100-m depth.

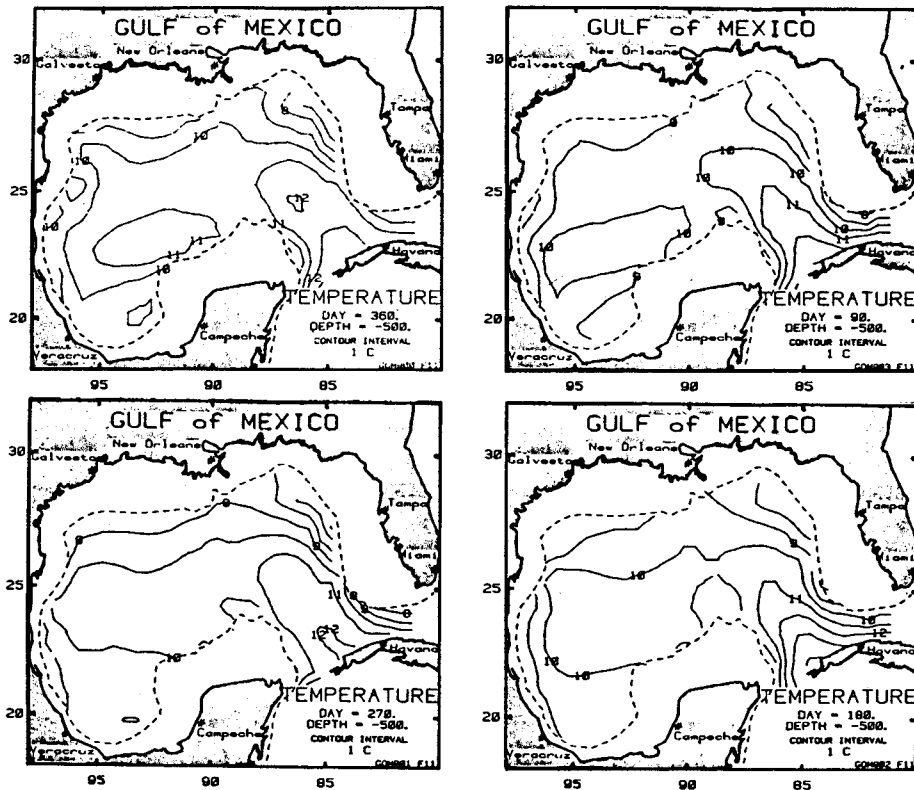


Fig. 9c. Same as Fig. 9a but for the 500-m depth.

evident at the 100-m depth level. The observations of Nowlin (1972) and Merrell and Morrison (1981) carry a hint of this upwelling. The model overpredicts both the temperature and salinity fields at 500 m by 1.5°C and 0.25‰ respectively. This may be due to the downwelling associated with the anticyclonic gyre so persistent in the western Gulf. On the other hand, the model reproduces the existing summer upwelling regions along the northern and western coasts of Yucatan. The model is also successful in predicting the rapid diminishing of large scale horizontal gradients as depth increases.

It is useful to reduce the large amount of information produced by the model by considering area-averaged, seasonal thermal variability of the upper Gulf layers, as in Figure 11a. Generally the model predicts the observed deepening and subsequent rapid rising of the isotherms over the course of the annual heating cycle. The results do not, however, show enough deepening. The timing of the onset of spring heating is also not well reproduced. Both of these discrepancies can be attributed to model start-up. The geostrophic adjustment tends to bring the initially tilting isotherms to a more horizontal

position where they have less potential energy. Thus the surface layers are cooled while the deeper layers are warmed immediately after initialization. In Figure 11a it appears that the 100-m or the 21°C isotherm separates the layers. After the adjustment occurs the model then begins to recover towards climatology. As a consequence of this experience the model is now routinely initialized with the results of a diagnostic run as in Blumberg and Mellor (1983).

The global averages of temperature and salinity are depicted in Figure 11b as a function of time for both data and model predictions. The model seems to have coped well with the initial adjustment processes as the global integrals, for the most part, follow climatology. The salinity cycle is reproduced, but the global temperature predictions show a distinct warming trend. An analysis of the model heat budget indicates that the Gulf acted as a heat sink to the atmosphere because of the feedback contribution ($+62\text{ Wm}^{-2}$) producing a net of $+14\text{ Wm}^{-2}$ when combined with the data-determined heat flux (-48 Wm^{-2}). The model is in effect being driven by a combination of data-determined heat flux and surface temperature. The advective heat flux (net heat

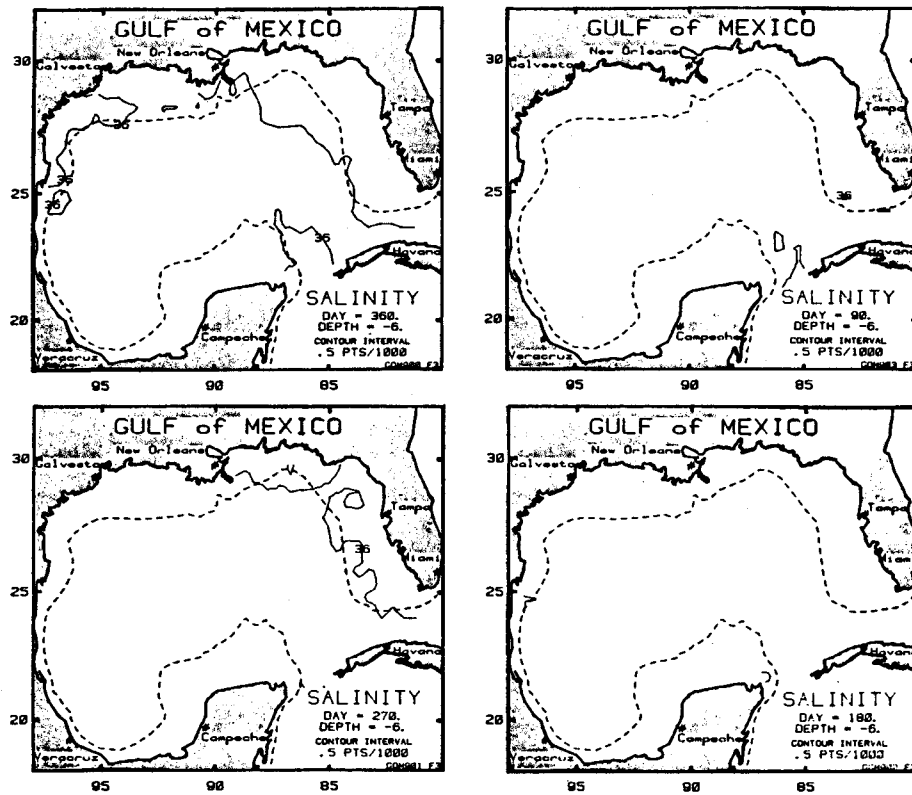


Fig. 10a. Calculated salinity distributions at 6 m below the surface. The sequence is clockwise and the middle day of the months May, August and November are shown. The initial condition on February 15 is that of Fig. 5 for January, February and March. The field shown here for February (15th) is the final calculated field.

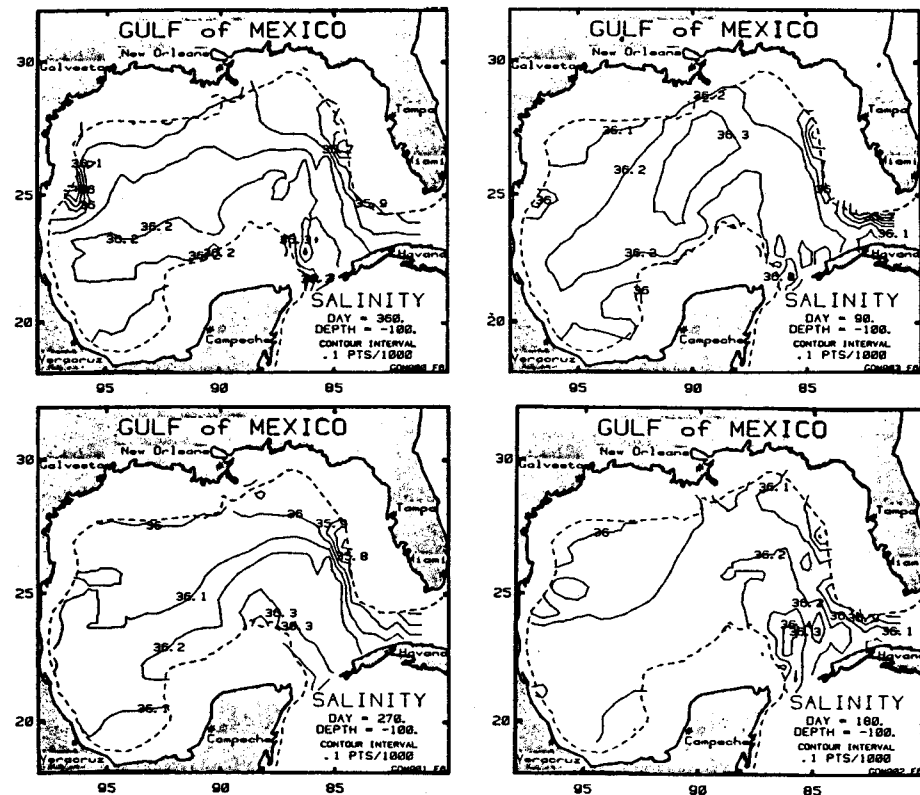


Fig. 10b. Same as Fig. 10a but for the 100-m depth.

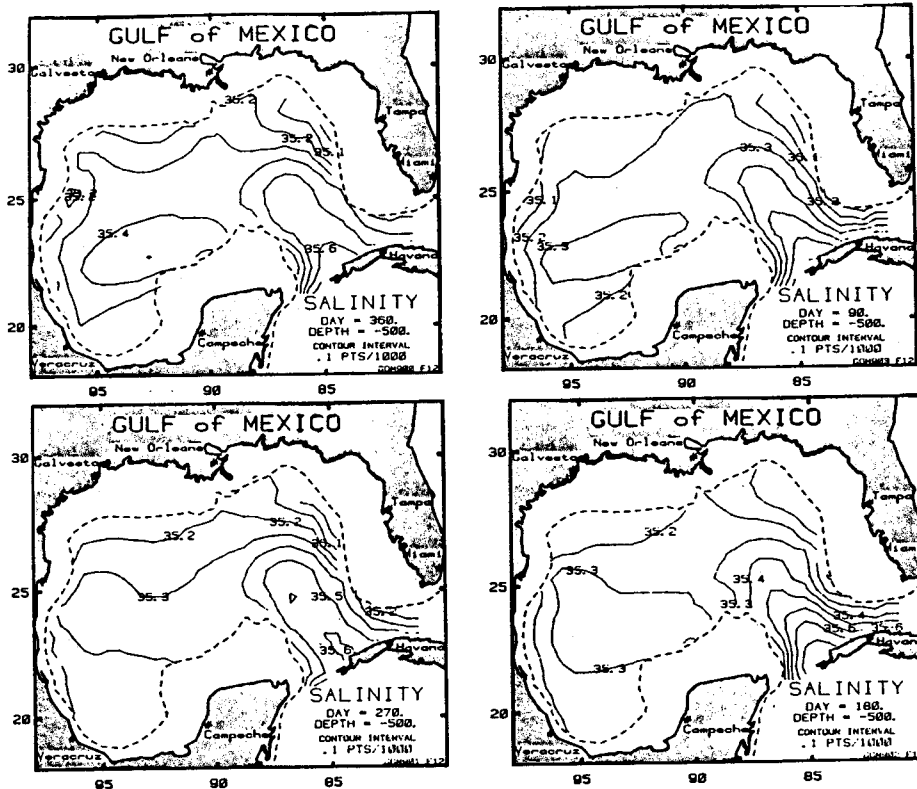


Fig. 10c. Same as Fig. 10a but for the 500-m depth.

transport by the currents divided by the surface area of the Gulf) was $+25 \text{ Wm}^{-2}$ and the rate of heat storage was, equivalently, 39 Wm^{-2} . The feedback contribution was significant because the start-up shock tended to cool the surface layers and made it seem, via the feedback terms, as if the Gulf required more heat input. The net advective flux, although within the estimates of Etter (1975), Hastenrath and Lamb (1978) and Bunker (1976), is probably responsible for the unobserved continued warming of the deeper waters. This indicates that the specification of the inflow/outflow boundary conditions should be subject to further detailed investigation.

In an attempt to understand the model's simulation of seasonal variability, numerical experiments have been conducted with a one dimensional model and therefore may be compared to the precursor work of Martin and Roberts (1977). The one-dimensional equations are the three-dimensional equations after averaging horizontally over the Gulf. The averaging procedure introduces terms such as those involving the net horizontal advection of heat into the basin and vertical velocity-temperature

correlations which are neglected in this analysis. The one-dimensional model employs the same wind model, vertical resolution, time step and initial conditions as the full model and is driven by the area-averaged atmospheric forcing data. The results from the experiment are shown in Figures 12 and 13. The resultant annual surface heat flux cycle (Figure 12) indicates as in the three-dimensional model that the feedback contribution alters the net flux as seen by the model Gulf. The annual means of the heat flux components from the $z-t$ model simulation are -48 Wm^{-2} from the analyzed data (see Section 2) and $+57 \text{ Wm}^{-2}$ from the feedback term; the net annual mean is $+9 \text{ Wm}^{-2}$.

The seasonal variation of the isotherm depths is shown in Figure 13. The simulation produces close agreement with data (Figure 11a, left side). The feedback mechanism, it seems for the $z-t$ model, affects only the timing of the seasonal heating and cooling transitions. An additional calculation with the latent heat contribution reduced by 25% so that the data now supports a $+3 \text{ Wm}^{-2}$ net annual heat flux (see Section 2) produced similar results. Both calculations

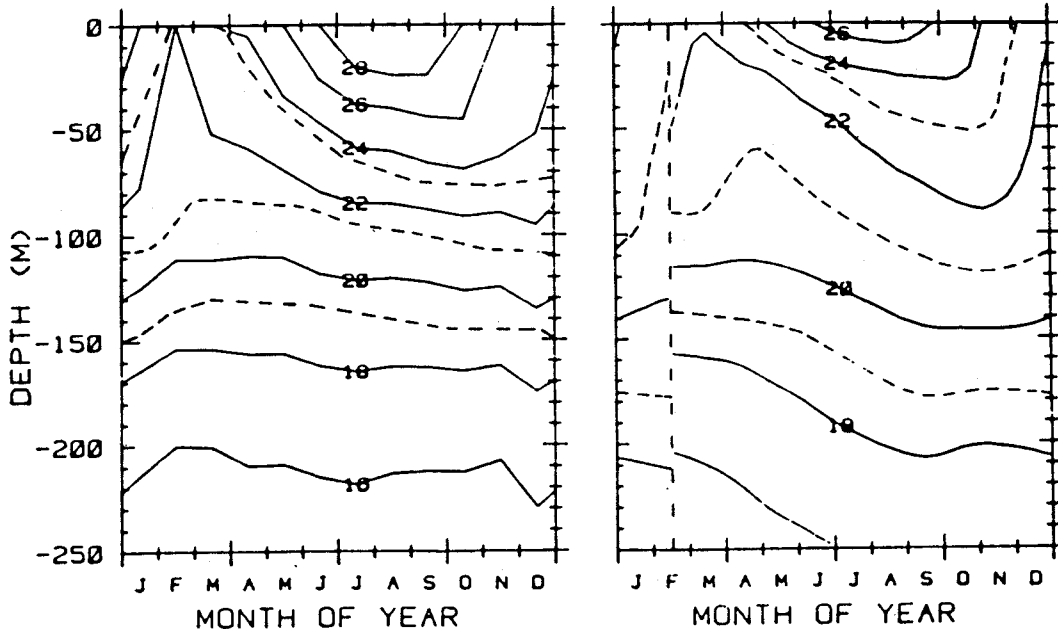


Fig. 11a. A comparison of the area-averaged observed temperature climatology (left) in the upper layers of the Gulf with the annual variation simulated by the numerical model (isotherms in °C). Dashed lines represent some of the odd valued isotherms. The model calculations began on February 15th.

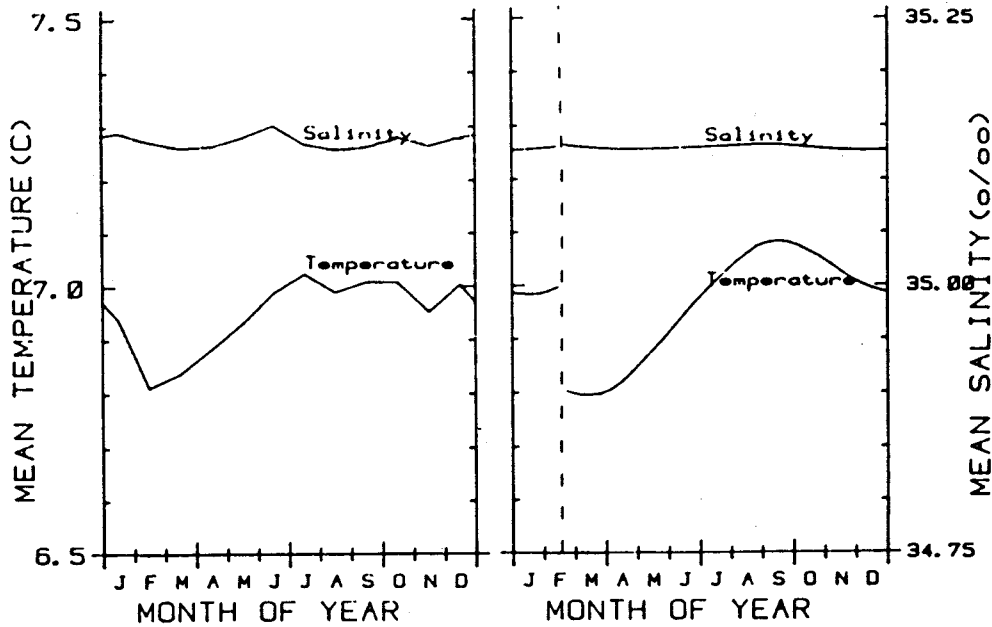


Fig. 11b. A comparison of the volume-averaged observed temperature and salinity climatology (left) of the Gulf with the annual variation simulated by the numerical model. The model calculations began on February 15th.

show little seasonal variability below 150 m. The slight deepening of the isotherms below this depth is due to the specified background mixing; the value $1 \times 10^{-4} \text{ m}^2 \text{ s}^{-1}$ is either too large at this depth or

compensatory upwelling should have been specified. Analogous numerical experiments conducted by Blumberg and Mellor (1979) employing a similar heat flux but a different wind model produced results

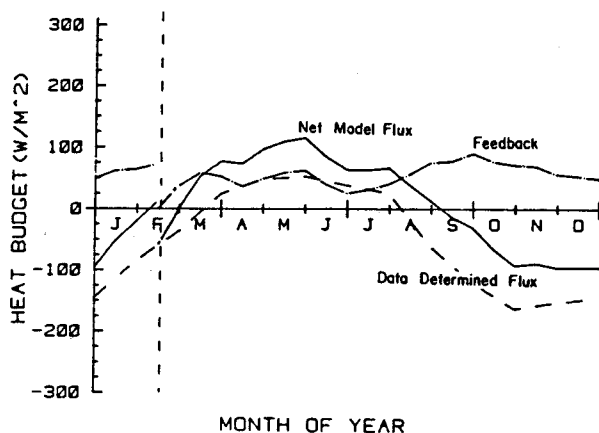


Fig. 12. The annual cycle of the heat flux components calculated by an area averaged ($z-t$) model of the Gulf. The model calculations began and ended on February 15th.

which differ in the upper 20 m from those discussed in this section. It seems that the application of a wind stress via a wind model in conjunction with a heating cycle containing transitions is a relatively delicate matter and may, if one were to consider individual years, govern the mixed-layer depth and surface temperature of the entire summer.

The result of the experiment (Figure 13) agrees better with the data than does the equivalent distribution produced by the full model (Figure 11a, right

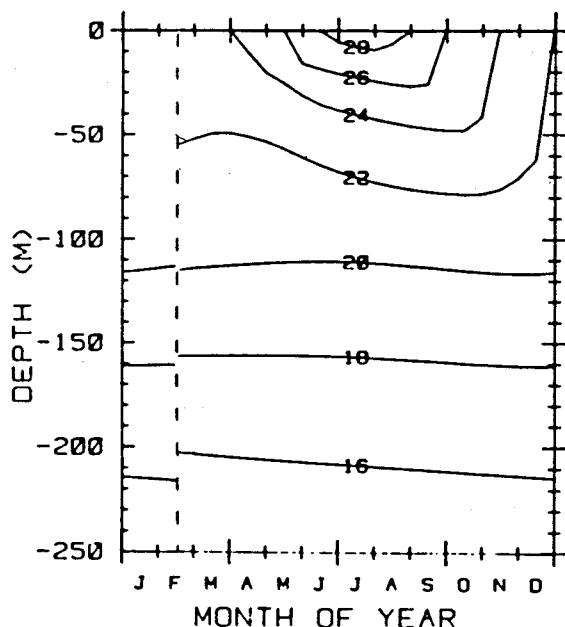


Fig. 13. The annual variation of temperature in the Gulf calculated by an area averaged ($z-t$) model. Isotherms in $^{\circ}\text{C}$. The model calculations began on February 15th.

side). The primary reason seems to be that the one-dimensional model has no initial geostrophic adjustments; the secondary reason applicable to the deeper waters is that there is no deep water warming caused by advection in the one-dimensional model.

Summary

The research efforts described in this paper were directed towards producing a realistic, although with somewhat coarse horizontal resolution, model of the dynamic and thermodynamic processes occurring in the Gulf of Mexico. An efficient three-dimensional, time-dependent prognostic model of the Gulf has been developed and used. The model is driven by winds and surface heat flux derived from climatological, atmospheric surface data, the result of an intensive data analysis study. Mean velocity, temperature, salinity, turbulence kinetic energy and turbulence macroscale are the prognostic variables. Lateral boundary conditions for temperature and salinity and geostrophically derived velocity at the Straits of Yucatan and Florida are obtained from climatological ocean data. An analytical second moment turbulence closure scheme embedded within the model provides realistic surface mixed layer dynamics. Free surface elevation distributions are calculated with an algorithm which calculates the external mode separately from the internal mode. The external mode, an essentially two-dimensional calculation, requires a short integrating timestep whereas the more costly, three-dimensional, internal mode can be executed with a long step. The result is a fully three-dimensional code which includes a free surface at only minimal sacrifice in computer cost compared to rigid lid models.

The results from a one year calculation appear, subjectively, to be a rather good simulation although the Loop Current does not shed large amplitude eddies. The horizontal coefficient of eddy viscosity and the horizontal resolution will probably have to be lowered before an intense eddy shedding instability will occur. Nevertheless smaller scale baroclinic eddies are evident throughout the simulation. The model does seem to reproduce much of the large scale features of the circulation such as the variability, intensity and areal extent of major current systems as construed from comparisons with available observational data. The seasonal variation of the mixed layer and thermocline compares well, but not perfectly, with climatology. The comparisons also reveal that in the future more attention should be

given to the details of model initialization. In general the fact that detailed deficiencies can be identified should lead to strategies for improved model simulations.

Acknowledgements

The authors wish to express thanks to Dr. H. James Herring, Dr. Lakshmi H. Kantha and Prof. Christopher N.K. Mooers for many enlightening discussions concerning this research effort. The atmospheric forcing climatology was compiled by Dr. Herring. Much of the credit for the production of this paper goes to Ms. Marianne L. LaRiche. This work was supported by the Division of Solar Technology, US Department of Energy under Contract Number DE-ACO2-78ET20612.

References

- Arakawa, A. and V.R. Lamb. 1977. Computational design of the basic dynamical process of the UCLA general circulation model. *Methods Comput. Phys.* 17: 173–265.
- Baer, L., L.C. Adams and S.I. Adelfang. 1968. Experiments in oceanic forecasting for the advective region by numerical modelling, Part 2, Gulf of Mexico. *J. Geophys. Res.* 73: 5091–5104.
- Behringer, D.W., R.L. Molinari and J.F. Festa. 1977. The variability of anticyclonic current patterns in the Gulf of Mexico. *J. Geophys. Res.* 82: 5469–5476.
- Blumberg, A.F. and G.L. Mellor. 1979. A whole basin model of the Gulf of Mexico. *Proc. 6th Annu. Conf. OTEC, Department of Energy, Washington, DC.*
- Blumberg, A.F. and G.L. Mellor. 1983. Diagnostic and prognostic numerical circulation studies of the South Atlantic Bight. *J. Geophys. Res.* 88: 4579–4592.
- Blumberg, A.F. and G.L. Mellor. 1985. A description of a three-dimensional coastal ocean circulation model. In: N. Heaps, ed. *Three-Dimensional Shelf Models, Coastal and Estuarine Sciences, Vol. 5. American Geophysical Union.*
- Brooks, D.A. and J.M. Bane, Jr. 1979. Gulf Stream deflection by a bottom feature off Charleston, South Carolina. *Science* 201: 1225–1226.
- Brooks, D.A. and R.V. Legeckis. 1982. A ship and satellite view of hydrographic features in the western Gulf of Mexico. *J. Geophys. Res.* 87: 4195–4206.
- Bunker, A.F. 1976. Computations of surface energy flux and annual air–sea interaction cycles of the North Atlantic Ocean. *Mon. Weather Rev.* 104: 1122–1140.
- Chew, F. 1974. The turning process in meandering currents. *J. Phys. Oceanogr.* 4: 27–57.
- Elliott, B.A. 1982. Anticyclonic rings in the Gulf of Mexico. *J. Phys. Oceanogr.* 12: 1292–1309.
- Etter, P.C. 1975. A climatic heat budget study of the Gulf of Mexico. M.Sc. thesis, Texas A&M University, College Station, 87 p.
- Etter, P.C. 1983. Heat and freshwater budgets in the Gulf of Mexico. *J. Phys. Oceanogr.* 13: 2058–2069.
- Franceschini, G.A. 1961. Hydrologic balance of the Gulf of Mexico. Ph.D. dissertation, Texas A&M University, College Station, 149 p.
- Fofonoff, N.P. 1962. Physical properties of sea–water. In: *The Sea, Vol. 1.* Interscience, p. 3–30.
- Hamm, D.P. and R.M. Lesser. 1968. Experiments in oceanic forecasting for the advective region by numerical modelling, Part 1, the model. *J. Geophys. Res.* 73: 5081–5089.
- Hastenrath, S.L. 1980. Heat budget of tropical ocean and atmosphere. *J. Phys. Oceanogr.* 10: 159–170.
- Hastenrath, S.L. and P. Lamb. 1978. *Heat Budget Atlas of the Tropical Atlantic and Eastern Pacific Oceans.* University of Wisconsin Press, 104 p.
- Holland, W.R. and A.D. Hirschman. 1972. A numerical calculation of the circulation in the North Atlantic Ocean. *Phys. Oceanogr.* 2: 336–354.
- Hubertz, J.M., R.O. Reid and A. Garcia. 1972. Objective analysis of oceanic surface currents. In: L.R.A. Capurro and J.L. Reid, eds. *Contributions on the Physical Oceanography of the Gulf of Mexico, Vol. II.* Gulf Publishing Co., p. 139–148.
- Hurlburt, H.E. and J.D. Thompson. 1980. A numerical study of Loop Current intrusions and eddy shedding. *J. Phys. Oceanogr.* 10: 1611–1651.
- Hurlburt, H.E. and J.D. Thompson. 1982. The dynamics of the Loop Current and shed eddies in a numerical model of the Gulf of Mexico. In: J.C.J. Nihoul, ed. *Hydrodynamics of Semi-Enclosed Seas.* Elsevier Publishing Co., p. 243–298.
- Ichiye, T. 1962. Circulation and water mass distribution in the Gulf of Mexico. *Geofis. Int. (Mexico City)* 2: 47–76.
- Jacobs, W.C. 1951. The energy exchange between sea and atmosphere and some of its consequences. *Bull. Scripps Inst. Oceanogr.* 6(2): 27–122.
- Jones, J.I. 1973. Physical oceanography of the northeast Gulf of Mexico and Florida continental shelf area. In: J.I. Jones, R.E. Ring, M.O. Rinkel and R.E. Smith, eds. *A Summary of Knowledge of the Eastern Gulf of Mexico.* State University System of Florida, St. Petersburg, Florida, IIB-1-IIB-69.
- Kantha, L.H., A.F. Blumberg, H.J. Herring and G.L. Mellor. 1981. The physical oceanographic and sea surface flux climatology of the South Atlantic Bight. *Dynalysis of Princeton Report No. 70, Princeton, NJ.*
- Kirwan, A.D., Jr., G. McNally, M.S. Chang and R.L. Molinari. 1975. The effect of wind and surface currents on drifters. *J. Phys. Oceanogr.* 5: 361–368.
- Klein, P. 1980. A simulation of the effects of air–sea transfer variability on the structure of marine upper layers. *J. Phys. Oceanogr.* 10: 1824–1841.
- Leipper, D.F. 1970. A sequence of current patterns in the Gulf of Mexico. *J. Geophys. Res.* 75: 637–657.
- Martin, P.J. and G.O. Roberts. 1977. An estimate of the impact of OTEC operation on the vertical distribution of heat in the Gulf of Mexico. *Proc. 4th Annu. Conf. OTEC, Department of Energy, Washington, DC.*
- Maul, G.A.. 1979. The 1972–1973 cycle of the Gulf Loop Current, Part II: mass and salt balances of the basin. *FAO Fish. Rep. No. 200: 597–619.*
- Mellor, G.L. and T. Yamada. 1982. Development of a turbulence closure model for geophysical fluid problems. *Rev. Geophys. Space Phys.* 20: 851–875.

- Merrell, W.J. and J.M. Morrison. 1981. On the circulation of the western Gulf of Mexico with observations from April 1978. *J. Geophys. Res.* 86: 4181-4185.
- Miyakoda, K., R.F. Strickler and J. Chludzinski. 1978. Initialization with the data assimilation method. *Tellus* 30: 32-54.
- Molinari, R.L., F.J. Festa and D.W. Behringer. 1978. The circulation in the Gulf of Mexico derived from estimated dynamic height fields. *J. Phys. Oceanogr.* 8: 987-996.
- Munk, W.H. 1950. On the wind-driven ocean circulation. *J. Meteorol.* 7: 79-93.
- Niiler, P.P. and W.S. Richardson. 1973. Seasonal variability of the Florida current. *J. Mar. Res.* 31: 144-167.
- Nowlin, W.D. 1972. Winter circulation patterns and property distributions.: In: L.R.A. Capurro and J.L. Reid, eds. *Contributions on the Physical Oceanography of the Gulf of Mexico*, Vol. II. Gulf Publishing Co., p. 3-51.
- Nowlin, W.D., Jr. and H.J. McLellan. 1967. A characterization of the Gulf of Mexico waters in winter. *J. Mar. Res.* 25: 29-59.
- Paskausky, D.F. and R.O. Reid. 1972. A barotropic prognostic numerical circulation model. In: L.R.A. Capurro and J.L. Reid, eds. *Contributions on the Physical Oceanography of the Gulf of Mexico*, Vol. II. Gulf Publishing Co., p. 163-176.
- Reid, R.O. 1972. A simple dynamic model of the Loop Current. In: L.R.A. Capurro and J.L. Reid, eds. *Contributions on the Physical Oceanography of the Gulf of Mexico*, Chap. 9. Gulf Publishing Co., p. 157-159.
- Simons, T.J. 1974. Verification of numerical models of Lake Ontario: Part I. Circulation in spring and early summer. *J. Phys. Oceanogr.* 4: 507-523.
- Sturges, W.A. and J.P. Blaha. 1976. A western boundary current in the Gulf of Mexico. *Science* 192: 367-369.
- Wert, R.T. and R.O. Reid. 1972. A baroclinic prognostic numerical circulation model. In: L.R.A. Capurro and J.L. Reid, eds. *Contributions to the Physical Oceanography of the Gulf of Mexico*, Vol. II. Gulf Publishing Co., p. 177-209.